Towards Safer Obstacle Avoidance for Continuum-Style Manipulator in Dynamic Environments*

Ahmad Ataka[1], Peng Qi[2], Ali Shiva[1], Ali Shafti[1], Helge Wurdemann[3], and Kaspar Althoefer[1]

***Abstract*— The flexibility and dexterity of continuum manipulators in comparison with rigid-link counterparts have become main features behind their recent popularity. Despite of that, the problem of navigation and motion planning for continuum manipulators turns out to be demanding tasks due to the complexity of their flexible structure modelling which in turns complicates the pose estimation. In this paper, we present a real-time obstacle avoidance algorithm for tendon-driven continuum-style manipulator in dynamic environments. The algorithm is equipped with a non-linear observer based on an Extended Kalman Filter to estimate the pose of every point along the manipulator's body. A local observability analysis for the kinematic model of the manipulator is also presented. The overall algorithm works well for a model of a single-segment continuum manipulator in a real-time simulation environment with moving obstacles in the workspace of manipulators, able to avoid the whole body of manipulators from collision.**

I. Introduction

During the last decade, continuum manipulators, mostly inspired by biological properties of snake [1] or octopus [2], have become an emerging technology in robotics. Diverse continuum manipulators design and structures have been explored recently [3], [4], [5]. Researches on modeling and control have also been reported and summarized in [6], [7].

The flexibility and dexterity of such manipulators in comparison with rigid-link counterparts become main features behind their recent popularity. Their inherent bending ability makes them more suitable to be applied in cluttered environments such as surgery, or other medical applications [8]. In industry, continuum manipulators mounted on mobile platforms will have more flexibility than their industrial counterparts. Managing this flexibility, while still achieving speed and efficiency, is an important problem.

Despite of all this favorable features, the problem of modelling and pose estimation of continuum manipulators turns out to be daunting tasks due to their highly flexible structure.

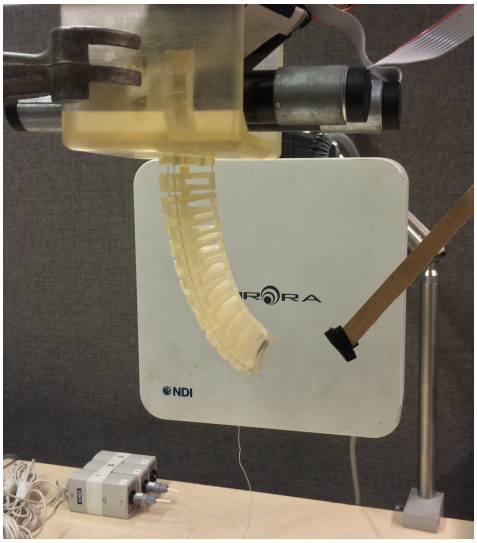

Fig. 1. A tendon-driven single-segment arms used as a model in this paper. To measure the tip's pose and the obstacle's pose, the NDI Aurora tracker can be adopted.

These will lead to a challenging problem of obstacle avoidance in which the whole body of manipulators needs to be kept safe from colliding with the surrounding environment, especially when the environment of the manipulators changes over time in an unpredictable way. Therefore, to have a real-time pose estimation strategy, combined with reactive obstacle avoidance, is crucial to achieve safe collision-free motion in dynamic environments.

Researches on continuum manipulators pose estimation have been reported in recent years. Most of the works have been implemented for snake-like robots [9], [10], [11]. Others used pose estimation to steerable catheter [12] and tendon-driven manipulators [13], [14]. Among other estimation techniques, the Kalman-Filter [9], [11] or a variance [15] have been predominantly employed. From the sensor side, various type of measurement strategy have been reported, such as inertial sensor [10] and visual sensing approach [15], [12], [14]. While the inertial sensor suffers from an accumulated integration error, visual sensing approach can be unreliable for dynamically changing environment. Other emerging approach in this field is the application of electromagnetic based sensor to track the position and orientation of a point on the robots body [9], [11]. Yet, the current researches lack a further utilization of the pose estimation approach to improve safety of continuum manipulators from collision.

*Research is partially supported by the STIFF-FLOP project grant from the European Commission Seventh Framework Programme under grant agreement 287728, the Four By Three grant from the European Framework Programme for Research and Innovation Horizon 2020 under grant agreement no 637095, and the Indonesia Endowment Fund for Education, Ministry of Finance Republic of Indonesia.

[1]Ahmad Ataka, Ali Shiva, Ali Shafti, and Kaspar Althoefer are with The Centre for Robotics Research (CoRe), Department of Informatics, Kings College London, London WC2R 2LS, United Kingdom. Corresponding author e-mail: ahmad.ataka@kcl.ac.uk

[2]P. Qi is with the Department of Biomedical Engineering, Faculty of Engineering, National University of Singapore, Singapore 117583. (e-mail: peng.qi@nus.edu.sg)

[3]H. Wurdemann is with the Department of Mechanical Engineering, University College London, Torrington Place, London WC1E 7JE, United Kingdom. (e-mail: h.wurdemann@ucl.ac.uk)

Corresponding author e-mail: ahmad.ataka@kcl.ac.uk

Preprint submitted to 6th IEEE RAS/EMBS International Conference on Biomedical Robotics and Biomechatronics. Received March 1, 2016.

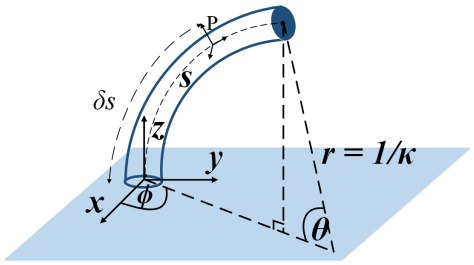

Fig. 2. The frame configuration used for a segment of the manipulator. A point P located at δs along the backbone can be expressed with the help of the scalar $\xi = \delta$.

For unpredictable dynamically changing environment, a real- time reactive obstacle avoidance is needed. Several obstacle avoidance approaches have been implemented in the field of continuum robot. A real-time adaptive motion planning approach was used for octopus-inspired continuum manipulator with moving obstacles [16]. However, the manipulator is assumed to move in planar case only while, at the same time, the algorithm has yet to produce solution in actuator space, limiting its application. An alternative work used an inverse-Jacobian-based planning to yield solutions in actuator space [17]. Yet, the avoid-obstacle approach is designed for a specific workspace inside a tubular environment. A well-known potential field method was successfully implemented for a steerable needle in soft tissue environment [18]. Although having a well-documented local minima problem, the reactive property of this approach makes it perfectly suited for dynamic environments.

In this paper, we propose a real-time obstacle avoidance for tendon-driven continuum manipulator in dynamic environments. The obstacle avoidance algorithm is derived from classical potential field and modified to be used in the kinematic model of continuum manipulators. An electromagnetic-based sensor is assumed to provide the tip's position of the manipulators. To enhance the safety of the whole body of manipulators, the algorithm is equipped with a non-linear observer based on an Extended Kalman Filter to estimate the pose of every point along the manipulator's body based on the model and measurement data. To our knowledge, this is the first attempt which further utilizes the pose estimation stage for safety improvement in avoiding collision for tendon-driven continuum manipulator. A local observability analysis for the kinematic model of the manipulator is presented. The overall algorithm is implemented for a kinematic model of a single-segment continuum manipulator as shown in Figure 2 [19]. The results illustrate the capability of the proposed algorithm to avoid collision in dynamically changing environments.

II. MODELLING OF CONTINUUM MANIPULATOR

A. Kinematic Model

Throughout this paper, we assume that the segment of the manipulator behaves like the arc of a circle with a constant radius of curvature. For manipulator whose workspace is in $\mathbb{R}^3$, the manipulator's segment can be specified by three configuration space variables $\mathbf{k} = \begin{bmatrix}\kappa & \phi & s\end{bmatrix}^T$ where κ, ϕ, and s denote the curvature, rotational deflection angle, and arc length of a segment respectively. By referring to Figure 1, the homogeneous transformation matrix describing the pose of the tip with respect to the base, $\mathbf{T}(\mathbf{k}) \in SE(3)$, is a function of the component of $\mathbf{k}$ as reported in [6].

$$\mathbf{T}(\mathbf{k}) = \begin{bmatrix} \cos\phi\cos\kappa s & -\sin\phi & \cos\phi\sin\kappa s & \frac{1}{\kappa}\cos\phi(1-\cos\kappa s) \\ \sin\phi\cos\kappa s & \cos\phi & \sin\phi\sin\kappa s & \frac{1}{\kappa}\sin\phi(1-\cos\kappa s) \\ -\sin\kappa s & 0 & \cos\kappa s & \frac{1}{\kappa}\sin\kappa s \\ 0 & 0 & 0 & 1 \end{bmatrix}. \quad (1)$$

Further mapping is needed to formulate the relationship between the previous configuration space variables $\mathbf{k}$ and the actuator space variables $\mathbf{q}$. This mapping depends on the manipulator's design and actuating mechanism. For a tendon-driven continuum manipulator, like the one presented in [19], a segment consists of three tendons whose length can be modified through the DC Motor system. Hence, the actuator space variables is specified by the length of each tendon and can be expressed as $\mathbf{q} = \begin{bmatrix} l_1 & l_2 & l_3 \end{bmatrix}^T$ where l_i represents the length of tendon-i. The relation between the configuration space variables $\mathbf{k}$ and the actuator space variables $\mathbf{q}$ is as follows [6]

$$\kappa(\mathbf{q}) = \frac{2\sqrt{l_1^2 + l_2^2 + l_3^2 - l_1 l_2 - l_2 l_3 - l_1 l_3}}{d(l_1 + l_2 + l_3)}. \quad (2)$$

$$\phi(\mathbf{q}) = \tan^{-1}\frac{\sqrt{3}(l_2 + l_3 - 2l_1)}{3(l_2 - l_3)}. \quad (3)$$

$$s(\mathbf{q}, \xi) = \frac{\xi \sum_{j=1}^{3} l_j}{3}. \quad (4)$$

where d represents the cross-section radius or the distance between the centre of the cross-section to each tendon and ξ is a scalar specifying a unique point located along the backbone of the manipulators. $\xi = 0$ stands for the base position and $\xi = 1$ stands for the tip of manipulator. Thus, any value of $\xi \in [0, 1]$ stands for a point locating between the base and the tip along the arc of the segment.

Hence, the complete forward kinematic relation can be expressed in the following form

$$\mathbf{T}(\mathbf{q}, \xi) = \begin{bmatrix} \mathbf{R}(\mathbf{q}, \xi) & \mathbf{p}(\mathbf{q}, \xi) \\ \mathbf{0}_{1\times 3} & 1 \end{bmatrix} \quad (5)$$

where $\mathbf{R}(\mathbf{q}, \xi) \in SO(3)$ denotes the rotation matrix and $\mathbf{p}(\mathbf{q}, \xi) \in \mathbb{R}^3$ denotes the position vector of the point along the body of manipulator.

A Jacobian of a point in the backbone of manipulator, $\mathbf{J}(\mathbf{q}, \xi) \in \mathbb{R}^{3\times 3}$, is defined as

$$\mathbf{J}(\mathbf{q}, \xi) = \frac{\partial \mathbf{p}(\mathbf{q}, \xi)}{\partial \mathbf{q}}. \quad (6)$$

It relates the velocity vector in the actuator space $\dot{\mathbf{q}}$ to the task space $\dot{\mathbf{p}}$ as follows

$$\dot{\mathbf{p}} = \mathbf{J}(\mathbf{q}, \xi)\dot{\mathbf{q}}. \quad (7)$$

Preprint submitted to 6th IEEE RAS/EMBS International Conference on Biomedical Robotics and Biomechatronics. Received March 1, 2016.

B. State-Space Representation

The state space representation is used to describe the kinematic model of the continuum manipulator. The state equation and output equation in discrete form are as follows

$$\mathbf{x}_{k+1} = f(\mathbf{x}_k, \mathbf{u}_k), \tag{8}$$

$$\mathbf{y}_k = g(\mathbf{x}_k), \tag{9}$$

where $\mathbf{x}_k \in X$, $\mathbf{u}_k \in U$, and $\mathbf{y}_k \in Y$ denote the state, input, and output value at iteration-k respectively while X, U, and Y denote the state space, input space, and output space respectively. The function $f : X \times U \to X$ is used to map the current state and input to the next state while $g : X \to Y$ is used to map the current state to the output.

For the kinematic model in Section II, the tendon's length $\mathbf{q} \in \mathbb{R}^3$ is used as a state variable $\mathbf{x}$. The actuator that we use in our manipulator is DC motor; each is connected to a tendon which will governs the pose of manipulator. So, our input signal $\mathbf{u}$ in this case is given by the DC motor's rotational speed which is identical to the tendon length's rate of change $\dot{\mathbf{q}} \in \mathbb{R}^3$.

$$\mathbf{x} = \mathbf{q} = \begin{bmatrix} l_1 & l_2 & l_3 \end{bmatrix}^T, \tag{10}$$

$$\mathbf{u} = \dot{\mathbf{q}} = \begin{bmatrix} \dot{l_1} & \dot{l_2} & \dot{l_3} \end{bmatrix}^T. \tag{11}$$

For the time sampling of Δt, the state equation in (8) can be rewritten as

$$\mathbf{x}_{k+1} = f(\mathbf{x}_k, \mathbf{u}_k) = \mathbf{x}_k + \Delta t \mathbf{u}_k. \tag{12}$$

To construct the output equation, we have to know what sensor is available in the manipulators. In this paper, we assume that a 3-DOF electro-magnetic-based tracker is embedded in the tip of manipulator. This sensor will give a position of the tip with respect to the base. The measurement rate is assumed to be identical to the sampling frequency $\frac{1}{\Delta t}$ such that new data is always available at every iteration. Therefore, the output $\mathbf{y}$ in Equation (9) is denoted by the tip's position with respect to the base, $\mathbf{p}$.

$$\mathbf{y} = g(\mathbf{x}_k) = \mathbf{p}(\mathbf{q}, \xi = 1), \tag{13}$$

Thus, the output equation is a forward kinematics relation, i.e. it matches the component of the homogeneous transformation matrix in Equation (5).

Knowing the input value at every iteration $\mathbf{u}_k$ and the initial state $\mathbf{x}_0$, we can determine the value of the state $\mathbf{x}_k$ as well as the position of a point along the backbone of the manipulator $\mathbf{p}(\mathbf{q} = \mathbf{x}_k, \xi)$ at every iteration using Equation (12) and (5). However, the value of initial state $\mathbf{x}_0$ is usually unknown. Moreover, using only the state equation and forward kinematics relation, the error in choosing the initial state value will result in an error in the whole manipulator's pose estimation. This will in turn pose a problem for the motion planning stage to achieve the target position and avoid collision. To overcome this problem, a non-linear observer is needed to estimate the pose without relying on the information of the state's initial value.

III. THE PROPOSED OBSTACLE AVOIDANCE ALGORITHM

A. Observability Analysis of a Linearized Kinematic Model

Before designing the observer, it is important to check the system's observability. A linearization is used to check the local observability of a non-linear model. In this section, we present an observability analysis on a linearized version of the non-linear kinematic model presented in previous section.

A linear system can be expressed by the following state equation and output equation

$$\mathbf{x}_{k+1} = \mathbf{A}\mathbf{x}_k + \mathbf{B}\mathbf{u}_k, \tag{14}$$

$$\mathbf{y}_k = \mathbf{C}\mathbf{x}_k. \tag{15}$$

The linearization of a non-linear model is achieved by computing the corresponding matrix $\mathbf{A} = \frac{\partial f(\mathbf{x}_k, \mathbf{u}_k)}{\partial \mathbf{x}_k}$, $\mathbf{B} = \frac{\partial f(\mathbf{x}_k, \mathbf{u}_k)}{\partial \mathbf{u}_k}$ and $\mathbf{C} = \frac{\partial g(\mathbf{x}_k)}{\partial \mathbf{x}_k}$.

To check the observability, we only need matrix $\mathbf{A}$, which turns out to be an identity matrix, and $\mathbf{C}$, which turns out to be a Jacobian of the tip given by

$$\mathbf{A}_k = \frac{\partial f(\mathbf{x}_k, \mathbf{u}_k)}{\partial \mathbf{x}_k} = \mathbf{I} \in \mathbb{R}^{3\times 3}, \tag{16}$$

$$\mathbf{C}_k = \frac{\partial g(\mathbf{x}_k)}{\partial \mathbf{x}_k} = \frac{\partial \mathbf{p}(\mathbf{q}_k, \xi = 1)}{\partial \mathbf{q}_k} = \mathbf{J}(\mathbf{q}_k, \xi = 1). \tag{17}$$

Using Equation (6) and a chain-rule derivative, we can express the Jacobian matrix $\mathbf{J}(\mathbf{q}, \xi)$ as follows

$$\mathbf{J}(\mathbf{q}, \xi) = \frac{\partial \mathbf{p}(\mathbf{k}, \xi)}{\partial \mathbf{k}} \frac{\partial \mathbf{k}}{\partial \mathbf{q}} = \mathbf{J_k} \mathbf{J_q}. \tag{18}$$

The Jacobian matrices component are derived from Equation (1)-(4) as follows

$$\mathbf{J_k} = \begin{bmatrix} \frac{\cos\phi(\kappa s \sin \kappa s + \cos \kappa s - 1)}{\kappa^2} & -\frac{\sin\phi(1-\cos\kappa s)}{\kappa} & \cos\phi \sin \kappa s \\ \frac{\sin\phi(\kappa s \sin \kappa s + \cos \kappa s - 1)}{\kappa^2} & \frac{\cos\phi(1-\cos\kappa s)}{\kappa} & \sin\phi \sin \kappa s \\ \frac{\kappa s \cos \kappa s - \sin \kappa s}{\kappa^2} & 0 & \cos \kappa s \end{bmatrix} \tag{19}$$

$$\mathbf{J_q} = \begin{bmatrix} \frac{3(l_1 l_2 + l_1 l_3 - l_2^2 - l_3^2)}{d l_+^2 l_s} & -\frac{3(l_1^2 - l_1 l_2 - l_2 l_3 + l_3^2)}{d l_+^2 l_s} & -\frac{3(l_1^2 - l_1 l_3 - l_2 l_3 + l_2^2)}{d l_+^2 l_s} \\ \frac{\sqrt{3}(l_3 - l_2)}{2 l_s^2} & \frac{\sqrt{3}(l_1 - l_3)}{2 l_s^2} & \frac{\sqrt{3}(l_2 - l_1)}{2 l_s^2} \\ \frac{1}{3} & \frac{1}{3} & \frac{1}{3} \end{bmatrix} \tag{20}$$

where $l_+ = l_1 + l_2 + l_3$; $l_s = \sqrt{l_1^2 + l_2^2 + l_3^2 - l_1 l_2 - l_1 l_3 - l_2 l_3}$.

An observability matrix $\mathbf{O} = \begin{bmatrix} \mathbf{C} & \mathbf{CA} & \dots & \mathbf{CA}^{n-1} \end{bmatrix}^T$ can be used to check whether the system with n number of state is observable. For our linearized system, the observability matrix $\mathbf{O} \in \mathbb{R}^{9\times 3}$ is expressed as

$$\mathbf{O} = \begin{bmatrix} \mathbf{J}(\mathbf{q}_k, \xi = 1) & \mathbf{J}(\mathbf{q}_k, \xi = 1) & \mathbf{J}(\mathbf{q}_k, \xi = 1) \end{bmatrix}^T. \tag{21}$$

The condition for observability is $\text{rank}(\mathbf{O}) = n = 3$. From the above equation, the following proposition is concluded.

Proposition 1: The linearized system as described in (14)-(20) is observable at all state except the singular state.

Proof: From the form of the matrix $\mathbf{O}$, we can easily conclude that its rank is equal to the rank of the Jacobian matrix itself, i.e. $\text{rank}(\mathbf{O}) = \text{rank}(\mathbf{J}(\mathbf{q}, \xi))$. We can see from Equation (19)-(20) that each Jacobian component

Preprint submitted to 6th IEEE RAS/EMBS International Conference on Biomedical Robotics and Biomechatronics. Received March 1, 2016.

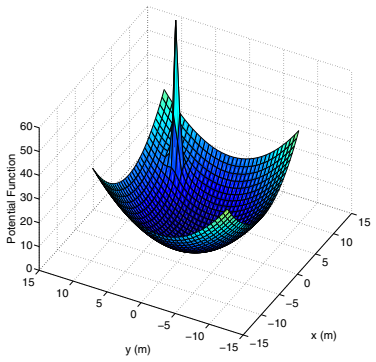

Fig. 3. Illustration of combined attractive and repulsive potential function applied in $\mathbb{R}^2$. The desired position is located at the lowest point of the potential while the high peak represents the obstacle's position.

(and equally their products) will always have a full rank aside from the singular configuration where $l_1 = l_2 = l_3$ and $\kappa = 0$ or a zero-bending configuration. Hence, if we assume that the manipulator is never at the singular configuration during the whole movement, both $\mathbf{J_k}$ and $\mathbf{J_q}$ will always have a full rank of $n = 3$, and so does matrix $\mathbf{O}$. So, the linearized system is concluded to be *observable* at every state except the singular configuration. ■

B. Pose Estimation

Knowing that the linearized system is observable, the well-known Extended Kalman Filter (EKF) is designed to estimate the state value, i.e. the tendon's length. From the state equation and output equation in (8)-(9), the EKF formulation is given by

$$\begin{aligned} \hat{\mathbf{x}}_{k+1|k} &= f(\hat{\mathbf{x}}_{k|k}, \mathbf{u}_k), \\ \mathbf{P}_{k+1|k} &= \mathbf{A}_k \mathbf{P}_{k|k} \mathbf{A}_k^T + \mathbf{Q}_k, \\ \mathbf{K}_k &= \mathbf{P}_{k+1|k} \mathbf{C}_k^T (\mathbf{C}_k \mathbf{P}_{k+1|k} \mathbf{C}_k^T + \mathbf{R}_k)^{-1}, \\ \hat{\mathbf{x}}_{k+1|k+1} &= \hat{\mathbf{x}}_{k+1|k} + \mathbf{K}_k (\mathbf{y}_k - g(\hat{\mathbf{x}}_{k+1|k})), \\ \mathbf{P}_{k+1|k+1} &= (\mathbf{I} - \mathbf{K}_k \mathbf{C}_k) \mathbf{P}_{k+1|k}. \end{aligned} \tag{22}$$

$\hat{\mathbf{x}}_{k+1|k+1}$, $\hat{\mathbf{x}}_{k|k}$, $\mathbf{u}_k$, and $\mathbf{y}_k$ stand for the next state estimation, the current state estimation, the input signal, and the measurement data respectively. The matrix $\mathbf{Q}_k \in \mathbb{R}^{3\times3}$ and $\mathbf{R}_k \in \mathbb{R}^{3\times3}$ denote the process noise variance and measurement noise variance respectively. The measurement $\mathbf{y}_k$ is taken from position sensor, such as an electro-magnetic based tracker, assumed to be embedded in the tip of manipulator. The pose estimation of the tip or any point along the segment of the manipulator can be derived by applying a forward kinematics in (5) to the state estimate $\hat{\mathbf{x}}$ produced by EKF. This pose information will be used in the obstacle avoidance.

C. Modified Potential Field

The obstacle avoidance algorithm employed in this paper is a modification of reactive potential field method [20]. The manipulator's workspace will be filled with a potential field, derived from a potential function U, designed to make tip of manipulator moves towards a defined target position while at the same time avoid the manipulator's body from collisions. The generalized potential field is derived from $\mathbf{F} = -\nabla U$.

A modification is made such that the standard potential field method can be applied to a kinematic model of a continuum manipulator. The generalized field $\mathbf{F}$ is regarded as the manipulator's velocity in task space, $\dot{\mathbf{p}}$. Therefore, $\dot{\mathbf{p}}$ is written as

$$\dot{\mathbf{p}} = -\nabla_{\mathbf{p}} U(\mathbf{p}). \tag{23}$$

An inverse Jacobian relation given in (7) is then used to get the actuator space velocity $\dot{\mathbf{q}}$ as the input to our system.

The attractive potential function is given by

$$U_d(\mathbf{p}) = \frac{1}{2} c (\mathbf{p} - \mathbf{p}_d)^T (\mathbf{p} - \mathbf{p}_d), \tag{24}$$

where $\mathbf{p}_d$ and c stand for a desired position and a positive constant gain respectively. The repulsive potential of an obstacle is given by

$$U_{\mathscr{O}}(\mathbf{p}) = \begin{cases} \frac{1}{2}\eta(\frac{1}{\rho} - \frac{1}{\rho_0})^2 & \text{if } \rho < \rho_0 \\ 0 & \text{if } \rho \geq \rho_0 \end{cases} \tag{25}$$

where $\rho = \sqrt{(\mathbf{p} - \mathbf{p}_{\mathscr{O}})^T (\mathbf{p} - \mathbf{p}_{\mathscr{O}})}$ represents the closest distance from an obstacle to the manipulator's body, η is positive constant, and ρ_0 denotes the limit distance of the potential influence.

The corresponding attractive velocity in workspace is given by

$$\dot{\mathbf{p}}_{\mathbf{p}_d} = -c(\mathbf{p} - \mathbf{p}_d). \tag{26}$$

The corresponding repulsive velocity can be calculated as follows

$$\dot{\mathbf{p}}_{\mathscr{O}} = \begin{cases} \eta(\frac{1}{\rho} - \frac{1}{\rho_0}) \frac{1}{\rho^2} \frac{\partial \rho}{\partial \mathbf{p}} & \text{if } \rho < \rho_0 \\ 0 & \text{if } \rho \geq \rho_0 \end{cases}. \tag{27}$$

Figure 3 shows an illustration of the potential function in planar case.

To make the whole body of the manipulator safe from any collision, a number of points, called *point subjected to potential* (PSP), is picked from the body of the manipulators. The closest PSP to the neighboring environment will be chosen as a point where the repulsive potential is applied. The pose of the tip ($\mathbf{p}(\mathbf{q}, \xi = 1)$) as well as the PSPs ($\mathbf{p}(\mathbf{q}, \xi \in [0,1])$) are all estimated by the EKF at every iteration as expressed by

$$\hat{\mathbf{p}}_k(\xi) = \mathbf{p}(\hat{\mathbf{x}}_{k|k}, \xi). \tag{28}$$

Lastly, the spatial velocity applied in the tip and the chosen PSP are mapped to the corresponding actuator space velocity and fed to the kinematic model as an input signal $\mathbf{u}_k$. The resulting velocity is given by a linear combination of attractive and repulsive velocity in actuator space as follows

$$\mathbf{u}_k = \dot{\mathbf{q}} = \mathbf{J}_e^{-1} \dot{\mathbf{p}}_{\mathbf{p}_d} + \mathbf{J}_a^{-1} \dot{\mathbf{p}}_{\mathscr{O}}. \tag{29}$$

$\mathbf{J}_e$ and $\mathbf{J}_a$ stand for the Jacobian of the tip and the chosen PSP respectively, as derived from (6) with the value of scalar ξ depending on the position of the PSP along the backbone of the manipulator. $\dot{\mathbf{p}}_{\mathscr{O}_b}$ corresponds to a repulsive potential produced by the closest obstacle.

Preprint submitted to 6th IEEE RAS/EMBS International Conference on Biomedical Robotics and Biomechatronics. Received March 1, 2016.

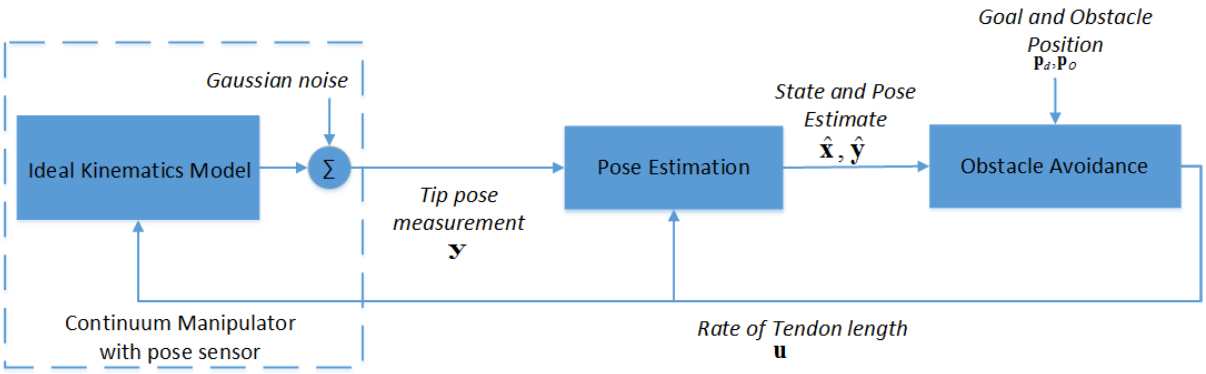

Fig. 4. The proposed pose estimator and obstacle avoidance algorithm. An ideal kinematics model, added with Gaussian noise, is used to replace the continuum manipulator and the pose sensor during the simulation.

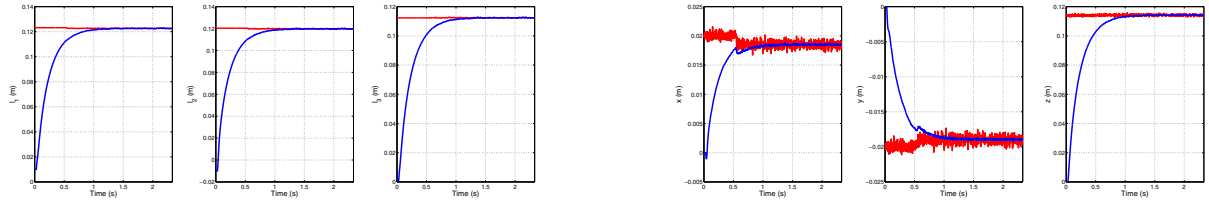

(a) (b)

Fig. 5. (a) The comparison between the true state (red line) and the estimated state (blue line) produced by the EKF for the zero-input scenario. (b) The comparison between the true pose with added Gaussian noise (red line) and the estimated pose (blue line) produced by the EKF for the zero-input scenario.

TABLE I
PROPERTIES OF MANIPULATOR, POSE ESTIMATOR, AND POTENTIAL FIELD

Param	Value	Param	Value
d	0.0134 m	c	2
$\mathbf{Q}$	$10^{-10}\mathbf{I} \in \mathbb{R}^{3\times3}$	η	2×10^{-9}
$\mathbf{R}$	$2.5\times10^{-7}\mathbf{I} \in \mathbb{R}^{3n\times3n}$	ρ_0	0.065 m
Δt	2.5×10^{-2} s		

Hence, we have combined the pose estimation and the obstacle avoidance algorithm to make the whole body of manipulators safer from collision. The overall algorithm is depicted in Figure 4.

IV. RESULTS AND DISCUSSION

Robot Operating System (ROS) real-time simulation environment was used to test the proposed algorithm. The frequency is chosen to be $\frac{1}{\Delta t}$ =40 Hz. A single segment manipulator used as a model has properties as described in Table I. To noise in the simulated measurement data is assumed to be Gaussian with zero-mean and the standard deviation $\sigma = 10^{-4}$. The corresponding variance matrix is then given by $\mathbf{R} = \sigma^2\mathbf{I} \in \mathbb{R}^{3\times3}$. Three PSPs are assumed to be located uniformly along the backbone of manipulators from the tip to the point close to the base. An obstacle, assumed to be spherical with 5 mm radius, moves at a constant speed in the surrounding of the manipulator.

A. State and Pose Estimation

In the pose estimation simulation, we assume to have measurement data of the tip pose $\mathbf{y}_k$ from an ideal kinematic model with added Gaussian noise. This is used to replace an electro-magnetic tracker assumed to be embedded in the tip of manipulator during the simulation for the state estimation in the EKF. This perfect kinematic model has a true state $\mathbf{x}_k$ updated at every iteration. This true state, however, is assumed to be unaccessible. The proposed algorithm will only capitalize the estimated states $\hat{\mathbf{x}}_k$ from the EKF.

In the first simulation, the input signal is chosen to be zero ($\mathbf{u} = \mathbf{0} \in \mathbb{R}^3$). Starting from a random initial state value, the EKF receives the measurement data of the tip pose $\mathbf{y}_k$ and starts to estimate the state value as shown in Figure 5a. Using this estimate of tendon length, by employing the forward kinematics, the tip pose is estimated. The comparison between the measured and the estimated tip pose is shown in Figure 5b. We can see that the EKF needs a reasonably small amount of time (around $t = 1$ s) to reach the true value both for the state and the tip pose. This is important since we want to use the state estimate value as an input to the motion planning stage. Hence, we expect the estimation error to be close to zero as soon as possible before the obstacle avoidance detects any obstacle around.

In the second simulation, a circular path is given as a reference for the manipulator's tip. Using an inverse Jacobian in (7), the varying input signal $\mathbf{u}_k$ is derived. The true state and tip pose measurement data will then vary over time. The

Preprint submitted to 6th IEEE RAS/EMBS International Conference on Biomedical Robotics and Biomechatronics. Received March 1, 2016.

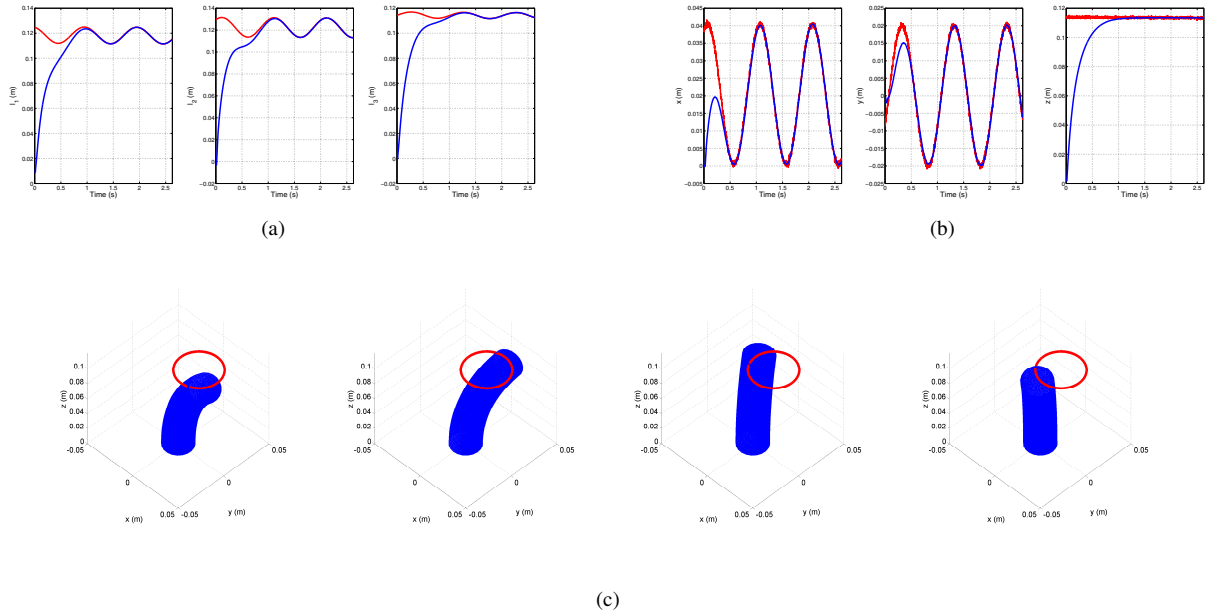

(a) (b)

(c)

Fig. 6. (a) The comparison between the true state (red line) and the estimated state (blue line) produced by the EKF for the circular-path scenario. (b) The comparison between the true pose with added Gaussian noise (red line) and the estimated pose (blue line) produced by the EKF for the circular-path scenario. (c) The movement of the continuum manipulator based on the estimated pose for circular-path scenario. The path is drew in red circle. The order of the movement is from left to right.

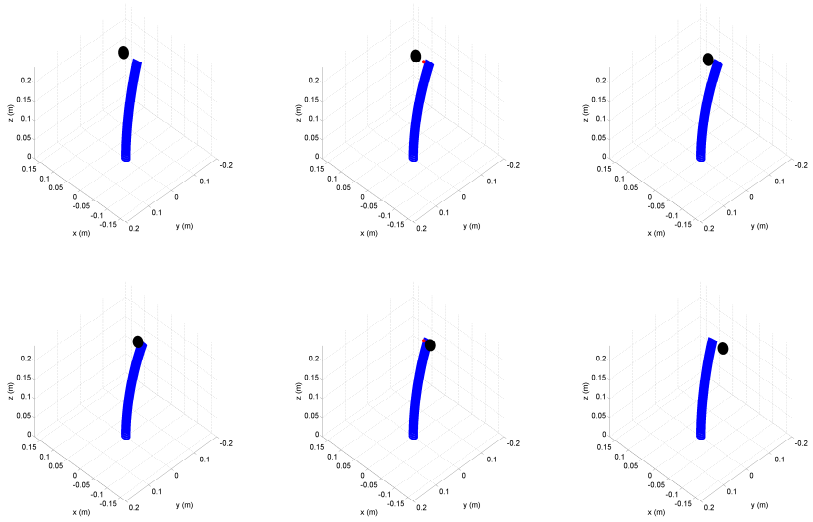

Fig. 7. The movement of the single segments continuum manipulator with a static target position (small red dot) when obstacle (black sphere) moves close to the tip of the manipulator. The order of movement is as follows: upper left picture, upper right picture, lower left picture, and finally lower right picture.

results, as depicted in Figure 6a and 6b, show that the EKF can cope with dynamically-changing input signal and tip pose's measurement. Figure 6c also shows the manipulator's movement estimation while tracking a red circular path.

B. Obstacle Avoidance

In this simulation, a pose estimator is used to estimate the pose of the tip and the PSPs along the body of manipulator to avoid obstacle and reach a desired target. The obstacle is drew as a black sphere while the tip's target, assumed to be fixed, is drew as a red dot.

In the first simulation, the obstacle moves at a height close to the tip's position as depicted in Figure 7. The obstacle avoidance works well, but the main contribution of the whole algorithm can be seen when the obstacle to move at a lower height, such as close to the manipulator's centre of mass as depicted in Figure 8. This height is chosen to check whether the proposed algorithm is capable of steering not only the tip but also the manipulator's body in a way that it is safe from collisions. Figure 8 shows how the obstacle avoidance stage exploits the pose estimation result to make the body of

Preprint submitted to 6th IEEE RAS/EMBS International Conference on Biomedical Robotics and Biomechatronics. Received March 1, 2016.

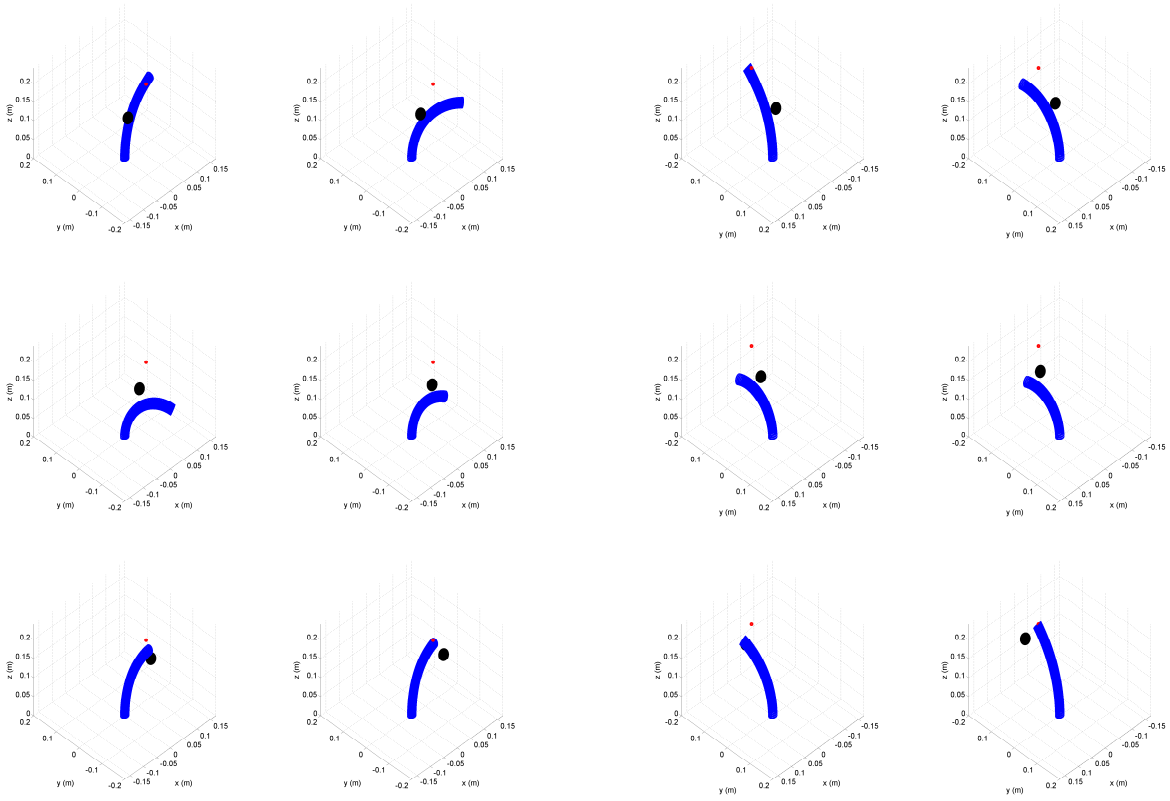

(a) (b)

Fig. 8. The movement of the single segments continuum manipulator with a static target position (small red dot) when obstacle (black sphere) moves close to the middle point of the manipulator's body (a) in x-axis direction and (b) y-axis direction. The order of movement for each subfigure is as follows: upper left picture, upper right picture, lower left picture, and finally lower right picture.

manipulator safer for the case of moving obstacle in x-axis direction (Figure 8a) and y-axis direction (8b).

C. Discussion

The simulation results show that the combined pose estimator and obstacle avoidance algorithm works well to keep a single segment continuum manipulator safe from collision in a real-time scenario with dynamic obstacle. One important assumption that we make is that the obstacle is still in a considerably large distance from the body of manipulator during the initial stage of estimation. This assumption is important because the pose estimate at that time, used in the motion planner stage, still does not match the real pose value due to the rise time needed by the EKF. Otherwise, the planner might produce a repulsive potential field which does not correspond to a real avoid-the-obstacle behavior. This can even disturb the performance of the pose estimator. This is another reason to keep the settling time and the rise time value of the error estimation dynamics as low as possible.

The results also illustrate that the proposed method can be implemented in a real manipulator. In that case, an electromagnetic tracker such as a 6-DOF NDI Aurora Tracker can be used to measure the tip's pose, as shown in Figure 1. Looking at these promising results, the proposed strategy can also be extended easily for a multi-segment continuum manipulator. In this case, we might need more than one electro-magnetic tracker to ensure the observability of the entire robot body.

Despite its fast execution time for real-time applications, the potential field itself is only a local reactive planner which does not guarantee completeness in complex environments. Running a global planner approach which produces an initial trajectory with global property on top of the reactive obstacle avoidance can also be explored in the future - this may, though, be too slow to provide suitable paths sufficiently quickly, especially in highly-dynamic environments.

V. Conclusions and Future Works

In this paper, a real-time pose estimator and obstacle avoidance for a tendon-driven continuum-style manipulator moving in dynamic environments is proposed. To our knowledge, this is the first attempt which combines together pose estimation and obstacle avoidance to improve the safety of a tendon-driven continuum manipulator, minimizing the risk of collisions between the manipulator body and obstacles in the robot workspace. The proposed algorithm is shown to perform in a real-time simulation.

This algorithm can be extended and applied to real manipulators, even in the case of multi-segment continuum

Preprint submitted to 6th IEEE RAS/EMBS International Conference on Biomedical Robotics and Biomechatronics. Received March 1, 2016.

arms. In the future, a more advanced dynamic model of the continuum manipulator can also be explored. A combination with a global motion planner approach when operating in more complex environments can also be designed.

REFERENCES

[1] S. Hirose, *Biologically inspired robots: snake-like locomotors and manipulators*, ser. Oxford science publications. Oxford University Press, 1993. [Online]. Available: https://books.google.co.uk/books?id=TaIQAQAAMAAJ

[2] W. McMahan, V. Chitrakaran, M. Csencsits, D. Dawson, I. Walker, B. Jones, M. Pritts, D. Dienno, M. Grissom, and C. Rahn, "Field trials and testing of the OctArm continuum manipulator," in *Robotics and Automation, 2006. ICRA 2006. Proceedings 2006 IEEE International Conference on*, May 2006, pp. 2336–2341.

[3] Y.-J. Kim, S. Cheng, S. Kim, and K. Iagnemma, "A Novel Layer Jamming Mechanism With Tunable Stiffness Capability for Minimally Invasive Surgery," *Robotics, IEEE Transactions on*, vol. 29, no. 4, pp. 1031–1042, Aug. 2013.

[4] T. Mahl, A. Hildebrandt, and O. Sawodny, "A Variable Curvature Continuum Kinematics for Kinematic Control of the Bionic Handling Assistant," *Robotics, IEEE Transactions on*, vol. 30, no. 4, pp. 935–949, Aug. 2014.

[5] F. Maghooa, A. Stilli, Y. Noh, K. Althoefer, and H. Wurdemann, "Tendon and pressure actuation for a bio-inspired manipulator based on an antagonistic principle," in *Robotics and Automation (ICRA), 2015 IEEE International Conference on*, May 2015, pp. 2556–2561.

[6] R. J. Webster, III and B. A. Jones, "Design and Kinematic Modeling of Constant Curvature Continuum Robots: A Review," *Int. J. Rob. Res.*, vol. 29, no. 13, pp. 1661–1683, Nov. 2010. [Online]. Available: http://dx.doi.org/10.1177/0278364910368147

[7] I. D. Walker, "Continuous backbone continuum robot manipulators," *ISRN Robotics*, vol. 2013, 2013.

[8] J. Burgner-Kahrs, D. C. Rucker, and H. Choset, "Continuum Robots for Medical Applications: A Survey," *IEEE Transactions on Robotics*, vol. 31, no. 6, pp. 1261–1280, Dec. 2015.

[9] S. Tully, G. Kantor, M. Zenati, and H. Choset, "Shape estimation for image-guided surgery with a highly articulated snake robot," in *Intelligent Robots and Systems (IROS), 2011 IEEE/RSJ International Conference on*, Sep. 2011, pp. 1353–1358.

[10] Z. Zhang, J. Shang, C. Seneci, and G.-Z. Yang, "Snake robot shape sensing using micro-inertial sensors," in *Intelligent Robots and Systems (IROS), 2013 IEEE/RSJ International Conference on*, Nov. 2013, pp. 831–836.

[11] R. Srivatsan, M. Travers, and H. Choset, "Using Lie algebra for shape estimation of medical snake robots," in *Intelligent Robots and Systems (IROS 2014), 2014 IEEE/RSJ International Conference on*, Sep. 2014, pp. 3483–3488.

[12] J. Borgstadt, M. Zinn, and N. Ferrier, "Multi-modal localization algorithm for catheter interventions," in *Robotics and Automation (ICRA), 2015 IEEE International Conference on*, May 2015, pp. 5350–5357.

[13] W. Rone and P. Ben-Tzvi, "Multi-segment continuum robot shape estimation using passive cable displacement," in *Robotic and Sensors Environments (ROSE), 2013 IEEE International Symposium on*, Oct. 2013, pp. 37–42.

[14] W. Xu, R. Foong, and H. Ren, "Maker based shape tracking of a flexible serpentine manipulator," in *Information and Automation, 2015 IEEE International Conference on*, Aug. 2015, pp. 637–642.

[15] E. Lobaton, J. Fu, L. Torres, and R. Alterovitz, "Continuous shape estimation of continuum robots using X-ray images," in *Robotics and Automation (ICRA), 2013 IEEE International Conference on*, May 2013, pp. 725–732.

[16] J. Xiao and R. Vatcha, "Real-time adaptive motion planning for a continuum manipulator," in *Intelligent Robots and Systems (IROS), 2010 IEEE/RSJ International Conference on*, Oct. 2010, pp. 5919–5926.

[17] G. Chen, M. T. Pham, and T. Redarce, "Sensor-based guidance control of a continuum robot for a semi-autonomous colonoscopy," *Robotics and Autonomous Systems*, vol. 57, no. 67, pp. 712 – 722, 2009. [Online]. Available: http://www.sciencedirect.com/science/article/pii/S0921889008002042

[18] S. DiMaio and S. Salcudean, "Needle steering and motion planning in soft tissues," *Biomedical Engineering, IEEE Transactions on*, vol. 52, no. 6, pp. 965–974, Jun. 2005.

[19] P. Qi, C. Qiu, H. Liu, J. Dai, L. Seneviratne, and K. Althoefer, "A novel continuum-style robot with multilayer compliant modules," in *Intelligent Robots and Systems (IROS 2014), 2014 IEEE/RSJ International Conference on*, Sep. 2014, pp. 3175–3180.

[20] O. Khatib, "Real-time obstacle avoidance for manipulators and mobile robots," in *Robotics and Automation. Proceedings. 1985 IEEE International Conference on*, vol. 2, Mar. 1985, pp. 500–505.

Preprint submitted to 6th IEEE RAS/EMBS International Conference on Biomedical Robotics and Biomechatronics. Received March 1, 2016.